A Hybrid CNN-LSTM Model for Flashover Alert on Polluted Insulators Using UHF and Acoustic PD Signals

Jorge Alfredo Ardila-Rey, Camilo Alvear Jorquera, Jorge Portilla Gómez, Bruno Albuquerque de Castro, Suganya Govindarajan and Luis Orellana

***Abstract*—Insulators are critical components in the transmission of electrical energy, and their correct operation is essential to guarantee the safety and continuity of the electrical supply. However, their constant exposure to environmental conditions such as pollution can affect their performance and lead to costly power outages. Proper monitoring and maintenance of this equipment are essential to avoid unexpected failures. Although significant progress has been made in the implementation of new monitoring methodologies and instruments, a solution that enables accurate and reliable online monitoring remains a challenge. This work presents a novel insulator flashover alert system that uses an acoustic sensor and an ultrahigh-frequency (UHF) antenna to detect partial discharge (PD) activity and generate alerts in three different states. The system uses hybrid deep learning models that combine a convolutional neural network (CNN) and a long short-term memory (LSTM) network that process the information provided by the sensors and generate local alerts to produce the general decision. This system can indicate whether the monitored insulator is in a normal state, an attention state, or an alarm state, which could help specialists take preventive measures and avoid sudden insulator failures.**

***Index Terms*—Acoustic measurement, deep learning, flashover analysis, insulators, partial discharge (PD), ultrahigh-frequency (UHF) measurement.**

I. Introduction

CERAMIC and nonceramic insulators have been widely used in electric power transmission and distribution systems, as well as in some high-voltage equipment. Their main function is to provide safe electrical insulation between live parts and the external environment [1], [2]. Although both types of insulators are designed to operate in environments where different degradation mechanisms are present, nonceramic insulators have been shown to deliver better performance in terms of aging [3], [4].

Regardless of the type of insulation that an insulator has, its geometry, or the voltage level applied, the electrical performance of these components will be strongly influenced by the extreme environmental conditions that are normally present in industrial, polar, desert, volcanic, or coastal areas, among others [1], [5]. The presence of polluting particles and traces of moisture found in this type of environment tends to form a conductive layer on the surface of the insulator that decreases the dielectric strength of the material over time. As a consequence, resistive leakage currents originate on the conductive layer, heating the insulator surface by the Joule effect, and evaporating the humidity until forming the so-called dry bands [6], [7]. The accumulation of electric charge at the edges of these bands, added to the applied electric field, can initiate a partial discharge (PD) activity that increases in magnitude and intensity over time, until finally the high flow of charges produces a complete discharge known as flashover. This event is the one that finally causes the equipment to go out of operation [1], [6], [8].

For this reason, the presence of PD is considered a relevant indicator when evaluating the general state of the insulators since the dynamics of these discharges change as surface contamination evolves. Despite the above, the behavior of PD cannot be generalized since the frequency of appearance, intensity, or spectral behavior of the signals (electric, ultrahigh frequency (UHF), or acoustic) will be different, even if the contamination process develops several times on the same type of insulator [9], [10].

Due to this, many power utility companies prefer to manage these assets based on the prioritization of maintenance needs and not on the actual condition of the equipment. For this prioritization, they resort to well-known methodologies in the technical literature, such as those proposed by Pareto and Jackknife [11], [12], [13], who use statistical data on maintenance and failures that occurred to establish the periodicity of the maintenance tasks, cleaning, and/or replacement.

This work was supported by the Agencia Nacional de Investigación y Desarrollo (ANID) Fondecyt regular 1230135 and Fondef TA24I10002. *(Corresponding author: Jorge Alfredo Ardila-Rey.)*

Jorge Alfredo Ardila-Rey and Camilo Alvear Jorquera are with the Department of Electrical Engineering, Universidad Técnica Fed-erico Santa María, Santiago 8940000, Chile (e-mail: jorge.ardila@usm.cl; camilo.alvear.14@sansano.usm.cl).

Jorge Portilla Gómez is with the Department of Electronics and Infor-matics Engineering, Universidad Técnica Federico Santa María, Concepción 4070317, Chile.

Bruno Albuquerque de Castro is with the Department of Electrical Engineering, School of Engineering, São Paulo State University (UNESP), Bauru 17033-360, Brazil (e-mail: bruno.castro@unesp.br).

Suganya Govindarajan is with the Kings College of Engineering, Pudukkottai 613303, India (e-mail: suganyasaravanan46@gmail.com).

Luis Orellana is with the Karlsruhe Institute of Technology (KIT), Institute for Pulsed Power and Microwave Technology (IHM), 76344 Eggenstein-Leopoldshafen, Germany (e-mail: luis.orellana@kit.edu).

Unfortunately, these methodologies can, in some cases, be inaccurate, leading to maintenance plans being overestimated or underestimated. This means that the reliability of the service and the economic resources are not properly optimized, generating, in some cases, problems in the electricity supply and economic losses for the companies themselves and/or consumers [14], [15].

In this context, the main challenge for companies and specialists in charge of maintenance is to be able to accurately predict or determine the level of contamination that the insulator has, or the moment in which the probability of flashover exceeds certain limits, so that necessary actions are taken to help prevent a sudden failure in the insulator [1], [6], [10]. Although, in recent years, important advances have been made in the development of new monitoring methodologies and instruments, implementing a solution of these characteristics remains highly challenging and complex, even more so when it comes to the development of online monitoring systems.

Different works, such as those presented in [16] and [17], use the leakage current as an indicator to measure surface degradation, insulation pollution severity, and insulator performance. The main problem with this variable is the electromagnetic interference that tends to alter the measurement process and the costs associated with the instrumentation that must be coupled to avoid losing sensitivity in the measurement. Techniques based on infrared (IR) and ultraviolet (UV) images [18], [19] have also been widely evaluated to monitor the level of contamination on the insulator surface. However, the images are limited to specific bands, which limits the information acquired from the insulator surface, in addition to the high costs of the equipment and instruments that are required for the measurements.

Other monitoring techniques that have also been explored in different works are acoustic techniques [4], [9], [14] and UHF [2], [20]. The acoustic techniques are based on measuring the mechanical waves generated by PD activity, while UHF techniques utilize antennas to capture the electromagnetic emissions produced by the charge flow on the insulator surface. In addition to their low sensor costs, both methods offer the advantage of not requiring direct electrical contact with the test object, enabling the instrumentation to be installed at any time without disconnecting the equipment. However, both acoustic and UHF techniques have their limitations, and neither has proven independently reliable in accurately predicting the precise moment of failure. Consequently, there is growing interest in developing hybrid systems that integrate at least two measurement methods [21]. The main advantage of this hybrid approach is the increased reliability of PD detection, as well as a better understanding of the characteristics needed to identify parameters that could potentially predict breakdowns [2], [4], [7].

Therefore, it is of great importance to continue developing and evaluating new data processing instruments and tools that make it possible to identify, in a general way, the different stages of the contamination processes in insulators. Among the most promising approaches to address this problem is the use of artificial intelligence (AI) algorithms, which have been shown to be highly efficient in classifying and identifying parameters for highly complex applications [4], [17], [19]. On the other hand, different studies have shown that the performance of these algorithms can be significantly improved if the input information comes from different types of sensors since the complementary variables obtained through multisensory systems allow AI techniques to broaden the spectrum of knowledge about the behavior of the phenomenon to be measured [22], [23]. To cover the abovementioned gap in the literature, this article presents a novel flashover warning system for insulators. The primary contributions are given as follows.

1) A measurement system that consists of an acoustic sensor and a UHF antenna that remotely captures PD activity.
2) The research proposes a decision-making approach using two artificial neural network (ANN) models, each combining a convolutional neural network (CNN) and a long short-term memory (LSTM) network. These models process sensor data independently to determine local alert states.
3) The general response of the system is developed to generate three distinct alert states, normal (no risk of flashover), attention (intermediate level of flashover probability), and alarm (high probability of flashover) based on the monitored insulator's condition, indicating varying levels of flashover risk.
4) This research also introduces a novel comparison of results through a series of ten offline and 17 online experiments conducted on a 34.5-kV ceramic insulator contaminated with saline solution, as opposed to conventional methods.

The structure of this article is detailed as follows. In Section II, the experimental setup and the methodology used to acquire signals through both types of sensors are described. Section III describes the architecture implemented for hybrid ANN models, their operation, and the decision logic used to generate the local response of the models and the general response of the system. The results obtained in the tests carried out both offline and online for different measurement processes are presented and discussed in Section IV. Finally, in Section V, the conclusions obtained from this research are detailed.

II. Materials and Methods

This section presents the experimental setup established to generate the datasets required for training, validating, and testing the proposed ANN models. The setup enables a controlled acquisition of PD sources through a UHF antenna and an acoustic sensor. By utilizing the UHF antenna, the electromagnetic emissions generated by PD are captured, while the acoustic sensor captures the corresponding mechanical waves. Once the information from both sensors was stored, a preprocessing step was carried out on every acoustic measurement dataset, allowing the extraction of the most relevant characteristics of the temporal and spectral responses of this sensor. Finally, with this information, the individual performance of the implemented hybrid models and the general response of the proposed system were evaluated.

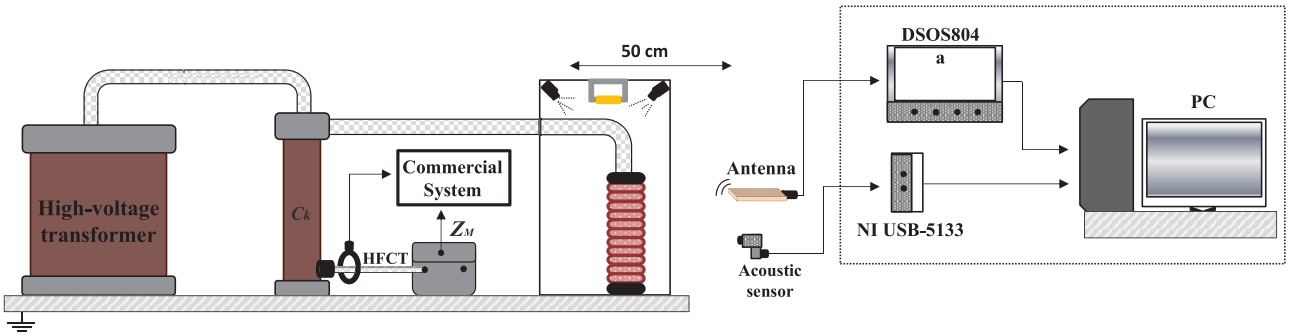

Fig. 1. Experimental setup for flashover tests.

A. Experimental Setup

Experimentally, an attempt was made to recreate in an accelerated way the contamination process that occurs in an insulator under normal operating conditions. For this purpose, a mixture of water with sodium chloride (NaCl) was used as a contaminating element (167 *g*/Lt). The contamination process was carried out by periodically spraying the surface of the insulator with the mixture while maintaining a constant voltage level. In this way, the salt deposit increased over time, until finally the necessary conditions were produced in the insulator so that flashover occurred. It is evident that the salt particles are not going to produce significant changes in the dielectric strength of the insulator by themselves; however, when these particles get wet or dissolve due to humidity, an ionic conductive solution is formed, which alters the electric field in different areas of the insulator, decreasing its dielectric strength and causing charge flows on the surface [24], [25].

For the PD generation and measurement process, a 34.5-kV nominal voltage ceramic insulator was used as the test object. To produce an initial deposit of salt on the surface of the insulator before starting the measurement process, the insulator was sprinkled with the polluting mixture through a manual sprayer and subsequently dried with an industrial dryer. As can be seen in Fig. 1, the test object is positioned inside an acrylic box that contains a halogen light in the upper part (in order to emulate the sun and the effect it exerts by accelerating the drying of moisture) and two manual sprinklers mechanically activated remotely (to avoid the electromagnetic noise normally generated when the sprayer is electric).

The sensors used for the measurement process correspond to a commercial Deepace KC R102 antenna and a commercial IPEC AA-Ultrasonic acoustic sensor. The antenna is of the open slot type, highly directional, and very efficient in the detection of electromagnetic radiation, depending on the direction in which the antenna is oriented. Although this antenna can capture spectral components in the entire UHF range, it is adapted to capture them with greater efficiency in the frequency range between 1500 and 2500 MHz. The emission of electromagnetic radiation from the PD pulses is in the range of 300 MHz and 2.5 GHz; therefore, the antenna is suitable for this type of application [26]. On the other hand, the acoustic sensor is a commercial sensor specially designed to detect the acoustic emissions that come from PDs [4]. This sensor's physical dimensions are $71 \times 37 \times 39$ mm, and it operates in the ultrasonic range, specifically at 40 kHz.

For the measurement processes in each experimental series, both sensors are remotely positioned 50 cm from the test object. Data are collected using two different acquisition systems. This approach is necessary because acoustic emissions are on the millisecond scale, and it is not possible to properly measure them simultaneously with the antenna, as UHF signals are on the tens to hundreds of nanoseconds scale. For this reason, the acoustic sensor signals are acquired with an NI USB-5133 card, using a time window of 100 ms and a maximum sampling frequency of 100 kHz. A Keysight Infiniium DSOS804a oscilloscope was used for the experimental series captured with the antenna, using a time window of 1 μs and a sampling frequency of 5 GS/s.

Finally, the generation of high voltage in the test object was carried out through an indirect circuit in accordance with the IEC 60270 standard. This circuit is made up of a 400-V/150-kV high-voltage transformer connected to the 220-V 50-Hz industrial network and controlled by a regulating transformer, as shown in Fig. 1. Likewise, the test object was connected in parallel to a low-impedance capacitive branch formed by a 1-nF capacitor (Ck) and a measurement impedance (Zm). In this way, a commercial PD system makes it possible to verify the presence or absence of PD sources at all times.

B. Signal Measurement and Pre-Processing

From the previous experimental setup, an adequate dataset was generated to train and test the hybrid ANN models that are part of the general decision system in charge of issuing the insulator flashover alert. In the case of the offline tests that will be described in Section IV, the measurement process of ten different experimental series was carried out, and the PD activity was captured with both types of sensors, also recording the time of occurrence of the signals with respect to the start of the experiment. Each measurement process started with a low level of danger since the salt deposited on the surface of the insulator at the beginning of the experiment was minimal. For this reason, during the first minutes of measurement, the PD activity captured by both sensors was low or null. As the experiment progressed, and the spraying processes were carried out (between 3 and 5 min), the PD activity evolved until finally, after a while, the flashover occurred, and moments later, the experiment was terminated. Table I shows the details of ten measurement processes carried out, where each one presented different flashover times despite the

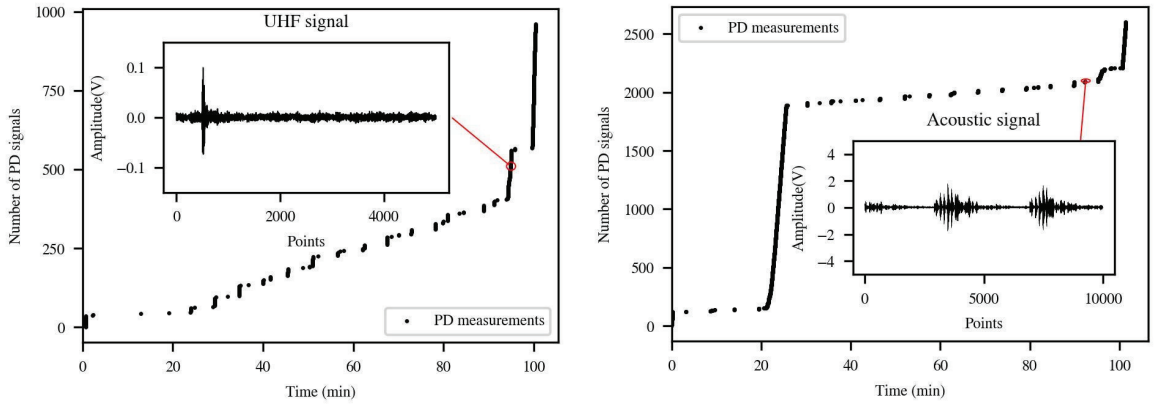

Fig. 2. Example of signals captured with both sensors during the measurement process of experimental series 3. (a) Pulse obtained with the antenna and (b) PD pulses obtained with the acoustic sensor.

TABLE I
INFORMATION ASSOCIATED WITH THE MEASUREMENT PROCESSES PERFORMED FOR THE OFFLINE TESTS

Experimental series	Number of UHF signals	Number of acoustic signals	Flashover (min)
1	1645	2500	68
2	1565	3200	180
3	985	2600	95
4	2745	13700	200
5	2775	3100	233
6	2220	1500	118
7	1430	13700	128
8	1395	16600	130
9	1535	30300	165
10	1200	12400	120

controlled conditions of the experiments. This validates the stochastic behavior of this degradation phenomenon.

It is worth noting that in a real scenario, the contamination process may be influenced by various factors, and the transition from a particular condition to a potential flashover could happen through multiple pathways [2], [3], [4], [8]. Nonetheless, this method effectively replicates the accumulation of contamination while enabling repeated experiments and obtaining an ample amount of data for the subsequent analysis.

Fig. 2 illustrates the measurement process for experimental series 3 described in Table I, which starts with a low PD activity in both sensors due to low levels of saline contamination. Subsequently, contamination levels rise until they reach a highly dangerous condition, and the flashover finally occurs at minute 95. For this case, the number of PD pulses obtained with the antenna was 985 with the antenna and 2600 with the acoustic sensor. Each measurement package captured with the UHF antenna corresponds to an array with dimensions $N \times 5000$, while, for the acoustic sensor, the array is set to $N \times 10\,000$, where N corresponds to the number of PD signals captured in each experiment

$$ru, v = hu, v * gu, v = n1 = -\infty\infty n2 = -\infty\infty hn1, n2gu - n1, v - n2. \quad (1)$$

Notably, there is no strict one-to-one correspondence between the pulses detected by the UHF antenna and those recorded by the acoustic sensor. This does not reflect a limitation of the measurement system but rather arises from the inherent physical differences between the sensors and the characteristics of the PD phenomenon itself. The UHF antenna is sensitive to extremely brief electromagnetic emissions and utilizes a 1-μs acquisition window per pulse, enabling detection of low-energy discharges, particularly in the early stages of contamination. By contrast, the acoustic sensor only responds to discharges whose mechanical energy is sufficient to generate a detectable ultrasonic wave, and it operates with a much wider acquisition window.

In addition, factors such as propagation delays, high event density, and the presence of ultrasonic and electromagnetic noise make an exact pulse-to-pulse alignment between sensors unfeasible, especially in long-term experiments. For this reason, the data from both sensors are grouped into analysis windows (five UHF PD pulses and ten acoustic PD pulses), allowing the models to learn from representative activity patterns rather than relying on individual pulse coincidences.

Before being used for the training of the UHF model, the UHF signals are normalized with respect to the maximum value established in the vertical adjustment of the oscilloscope used for the acquisition (800 mV). Likewise, the information provided by the acoustic sensor is preprocessed in order to extract relevant temporal and spectral information for the training and testing of the acoustic model. For this purpose, the envelope of each signal is calculated using the Hilbert transform, and the fast Fourier transform (FFT) of this envelope is obtained. As indicated in different works [4], [14], the information obtained with this type of sensor is contained in a carrier wave that changes according to the intensity and repetition rate of the mechanical waves generated

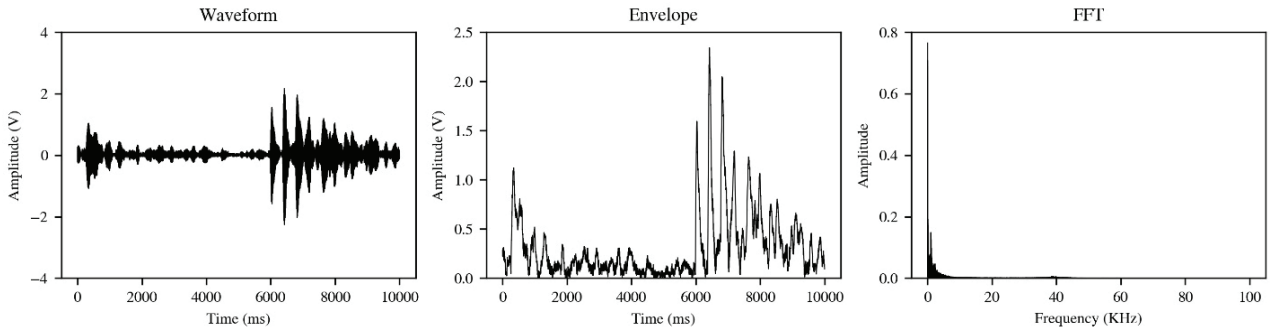

Fig. 3. Example of the preprocessing carried out on the acoustic signals prior to training, validation, and testing with the ANNs.

by PD activity at the insulator. With this preprocessing, the information delivered to the acoustic model will be specifically related to the global behavior of the mechanical waves coming from the PD signals. Fig. 3 shows one of the acoustic signals captured, the envelope obtained, and the FFT.

III. ANNs for Flashover Detection on a Polluted Insulator

This section describes the hybrid architecture of ANNs implemented for the acoustic and UHF models, the metrics used to evaluate the individual performance of each ANN model, and the operation of the proposed methodology for the general decision system.

A. Description of the Implemented Hybrid Architecture for the Acoustic and UHF Models

ANNs are adaptive structures that, upon receiving a dataset containing examples of input pairs and their corresponding output or ground truth, have the ability to adjust their internal parameters through a training process. In this way, they can model complex nonlinear relationships between inputs and outputs [27], [28], [29], [30].

In particular, CNNs are widely utilized for spatial processing of structured data, especially in image processing tasks. These networks consist of multiple layers designed to filter the input data and extract meaningful features from it, thereby capturing representative information. Convolutional layers apply a convolution operation on groups of close values of the input data to produce a new output array. The convolution operation is applied on sections of the input array $h(u, v)$ according to the size of the convolutional kernel or filter $g(u, v)$, which has a dimension no greater than $h(u, v)$ and is learned during training. The 2-D convolution operator between a kernel $g(u, v)$ and the input 2-D array $h(u, v)$ is formally defined as (1) [31], where u and v are the space coordinates. This kernel scrolls according to a slide value through the entire input array to produce the final output, which is a new array with extracted features. Each convolutional layer contains more than one kernel with parameters learned to extract different sets of features from the input.

On the other hand, it is important to highlight that LSTM networks are a type of recurrent neural network specifically designed to process sequential data series. These networks have an input layer, intermediate layers, and an output layer. In the intermediate layers, memory blocks known as "cells" are included. Each cell has three "gates": the input gate, the output gate, and the forget gate [32]. Each cell in an LSTM recurrent network is recurrently connected to these three inputs [33]. In different applications, CNN-LSTM models have been developed, merging convolutional layers to extract features from input data and LSTM layers to make sequence-based predictions. In general, the application of this type of model is oriented to the solution of problems of prediction or classification of time series, as is the case of the continuous activity of PD in insulators [34], [35].

The task of identifying the signals captured by the UHF antenna and the acoustic sensor poses a classification problem. The objective of the implemented algorithm is to provide an output that indicates if the signals analyzed represent a degree of danger that justifies the alert. To address this problem, a hybrid architecture that combines the advantages provided by CNN and LSTM networks is proposed as a solution. The main reason for using both topologies in time series applications is that CNNs are highly effective in extracting patterns or local features associated with the waveform of signals, while LSTMs can extract the information with great precision of temporal sequence patterns as PD activity evolves [27]. For this reason, it is expected that the hybrid architecture (CNN–LSTM) allows classifying the degree of hazard in the insulator due to its ability to efficiently extract the spatiotemporal characteristics of the analyzed signals.

Fig. 4 shows the ANN architecture proposed for the acoustic model. The model receives two inputs: one input corresponds to the preprocessed signals, and the other input corresponds to the time difference (Δ_t) of the consecutive PD signals. As indicated in Section II-B, the PD signals captured with the acoustic sensor are preprocessed and delivered to the model in groups of ten consecutive $10 \times 10\,000$ signals, which pass through a convolutional layer with 50 filters and a kernel size of 1×50, followed by a MaxPooling layer (1×10) and a dropout layer. Next, there is a flatten layer, which converts the multidimensional input into a 1-D representation. Up to this point, the layers described correspond to the time-distributed feature extractor, which extracts features from the waveform of the input signals. This information is condensed into a time-distributed layer (TDL), which means that those characteristics are determined for each signal in the group of ten signals. Likewise, the output of the time-distributed feature extractor is connected to a fully connected layer with 15 units

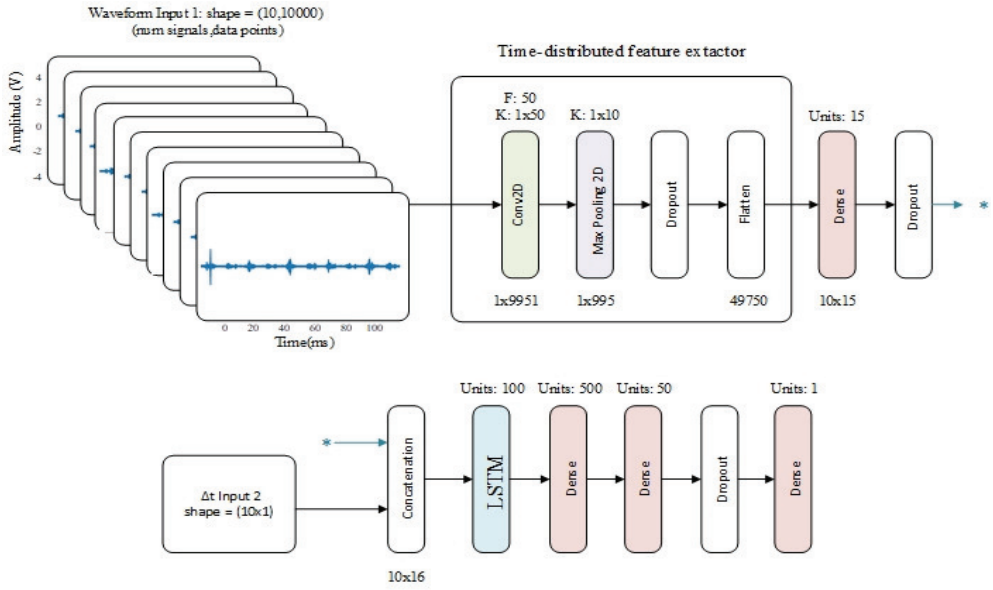

Fig. 4. Structure of the CNN-LSTM model proposed for the classification of the PD pulses captured with the acoustic sensor, where F and K correspond to the number of filters and the size of the kernel, respectively.

(10×15) and later to a dropout layer. The result obtained up to this point is concatenated with the sequence of time intervals (Δ_t with shape 10×1).

In the next stage, the network receives an input with dimensions 10×16, which passes through the LSTM layer that has 100 units. Two fully connected hidden layers (also known as dense layers) are then applied at 500 and 50 units, respectively. After the last dense layer, a new dropout layer is added. The hidden layers have an ReLU activation function, defined as $\text{ReLU}(x) = \max\{0, x\}$ [36], and an output layer consisting of a single neuron with a sigmoid activation function. The network propagates the input through the hidden layers until it reaches the output layer, generating a value in the range [0, 1] that represents the flashover probability. In addition, dropout layers were added in order to avoid overfitting in model training [37]. These dropout layers apply a process that consists of temporarily disconnecting a group of cells from the network according to a certain probability. In this case, a probability value of 0.5 was employed.

The same architecture used for the acoustic model was used for the UHF model, which receives two inputs: one with the data captured by the UHF antenna and the other with the time difference between consecutive PD signals. Unlike the acoustic model, the data supplied to the UHF model from the UHF antenna are not preprocessed. Table II presents a description of the network architecture used and the hyperparameters specifically adjusted for this model.

A grid search approach was employed to identify the optimal hyperparameter settings for each of the ANN models (both acoustic and UHF). This involved evaluating combinations of various factors, such as convolutional filter sizes, kernel dimensions, the number of LSTM units, dense layer configurations, dropout rates, and learning rates, while keeping the MaxPooling window size fixed at 1×10. The defined hyperparameter space was extracted from literature to establish plausible parameter values and domains [4], [34].

TABLE II

DESCRIPTION OF THE ARCHITECTURE PROPOSED TO CLASSIFY THE ACTIVITY OF PD SIGNALS IN THE UHF MODEL

	Type	Maps	Kernel /stride	Size	Activation
Input 1		-	-	5x5000	-
TDL	Conv2D	10	1x100/1	1x4901	ReLU
	Max.Pool	-	1x10/1	1x490	-
	Dropout	-	-	1x490	-
	Flatten	-	-	4900	-
Dense		20	-	5x20	ReLU
Dropout		-	-	5x20	-
Concatenation		-	-	5x21 (with Input 2 (5x1))	
LSTM		120	-	120	-
Dense		500	-	500	ReLU
Dense		100	-	100	ReLU
Dropout		-	-	100	
Dense		1	-	1	Sigmoid

A k-fold cross-validation procedure (k = 5) was integrated into the grid search to maximize generalization and minimize overfitting. In each iteration, five data partitions were used for training, validation, and test. During this process, the Adam optimizer and the binary cross-entropy loss function were employed for model training. Hyperparameter combinations were ranked according to their validation performance using the metrics defined in Section III-B.

Once the best hyperparameter set was identified, the final testing stage was conducted on UHF signal packages and acoustic signals that had not been used in training or validation. The Keras API facilitated design evaluation and fine-tuning.

B. Evaluation Metrics

The performance evaluation of the proposed models is conducted by comparing the inferred classes with the assigned

reference classes. To evaluate the performance of both models, some criteria commonly used to evaluate classification algorithms, such as precision, recall, and accuracy, were used [30], [33]. Thus, it was possible to evaluate the predictive capacity with the number of true positives (TPs), true negatives (TNs), false positives (FPs), and false negatives (FNs).

Precision represents the percentage of flashover alerts correctly issued by the classification model among all the cases identified as positive, with the aim of measuring the model's ability to not misidentify a negative signal as positive, and is expressed as follows:

$$\text{precision} = \frac{\text{TP}}{\text{TP} + \text{FP}}. \tag{2}$$

The recall criterion represents the rate of positive cases that the classifier correctly predicted, over all the positive cases in the data. This criterion measures the model's ability to find all the positive signals in the dataset, expressed as follows:

$$\text{recall} = \frac{\text{TP}}{\text{TP} + \text{FN}}. \tag{3}$$

The accuracy metric (Acc) indicates the proportion of observations correctly classified (both positive and negative) in relation to the total number of cases, expressed as follows:

$$\text{Acc} = \frac{\text{TP} + \text{TN}}{\text{TN} + \text{TP} + \text{FN} + \text{FP}}. \tag{4}$$

C. Description of the General Decision System

The methodology implemented for the alert system can be summarized in three stages.

1) Stage 1: During this stage, the measurement of the signals is carried out through the antenna and the acoustic sensor. To process these signals with neural network models, it is required that the UHF signals be acquired in groups of 5, and the acoustic sensor signals in groups of 10. These configuration values are determined after performing different tests on both models and selecting those that yielded the best results in the classification of signals according to the level of danger assigned (see Stage 2). For the acoustic model, the acoustic sensor signals are preprocessed before entering the neural network as indicated in Section II-B. Thus, the information from the acoustic sensor corresponds to the global behavior of acoustic emissions from PDs. The antenna signals are supplied from acquisition to the next stage without any kind of preprocessing (except the normalization process also described in Section II-B).

2) Stage 2: The information associated with both sensors is taken individually to train the two ANN models using the same hybrid architecture and adjusting the hyperparameters according to the type of signal. The models are trained to identify the PD activity from a low hazard to a high hazard condition. Since all the experiments on the insulator were carried out from a normal state until reaching flashover, the aim was for both models to learn (based on training examples) when the signals may indicate a risk of flashover. For this purpose, during the training, the signals of each experimental series were labeled according to a level of danger, where dangerous signals are those that begin to occur from a percentage of time (P) between the beginning of the measurement (t_0) until flashover occurs ($t_{\max}$). This means that signals before P are defined as class 0 (without danger), while signals after P are defined as class 1 (signals with danger)

$$y = \begin{cases} 1, & t > t_{\max}\, xP \\ 0, & \text{otherwise} \end{cases}. \tag{5}$$

As will be detailed in the experimental results described in Section IV, the value of P in both models must be adjusted according to the type of insulator and the performance of each sensor throughout the measurement processes.

3) Stage 3: As summarized in Fig. 5, in this last stage, the results of both models are used to establish the response of the alert system. Each model provides a danger index between 0 and 1. These indices are compared with respect to decision thresholds adjusted for each type of insulator depending on how sensitive the local response of the models is desired. For the first part of the experimental results described in Section IV and based on multiple tests carried out experimentally for the type of insulator used as the test object, the interval between 0 and 0.35 was selected as the one where the hazard indices of the models are considered as normal activity, that is, without danger. Between 0.35 and 0.8, it was considered an activity that should be paid attention to, indicating an intermediate risk, and higher than 0.8, it is an alarm or danger situation. In this way, the three possible local alert states for each model are defined as follows:

call alert states for each model

$$= \begin{cases} \text{Normal}, & 0.35 \geq f^*(x) \geq 0 \text{ or } 0.35 \geq g^*(x) \geq 0 \\ \text{Attention}, & 0.8 \geq f^*(x) > 0.35 \text{ or } 0.8 \geq g^*(x) > 0.35 \\ \text{Alarm}, & f^*(x) > 0.8 \text{ org}^*(x) > 0.8 \end{cases} \tag{6}$$

where $f^*(x)$ and $g^*(x)$ represent the signal assigned to the output by the acoustic and UHF models given an input x, respectively.

Finally, the logic that governs the general response of the alert system is based on the local alert states of both models. For the type of insulator used, it was initially established that if the local decision of both models is normal or at least one of them is attention, the general response of the alert system is a normal state (0). If the decisions of both models are in an attention state or at least one of them is in an alarm, then the general decision of the system is an attention state (1). The alarm state in the general response (2) only occurs if the local alert state of both models is in the alarm state.

Table III summarizes the general response of the alert system according to the possible local alert states in the models. It must be considered that the activity of PDs in the insulators is highly variable. In addition, there are completely random external events that can modify the behavior of the PD activity, so it is necessary to include a hysteresis that allows the system to return to a previous state. The established hysteresis is based on waiting for 20 successive decisions of the normal type to go down to this state from one of attention, 20 successive decisions of the attention type to go down to this state from one of alarm, and 40 successive decisions of the

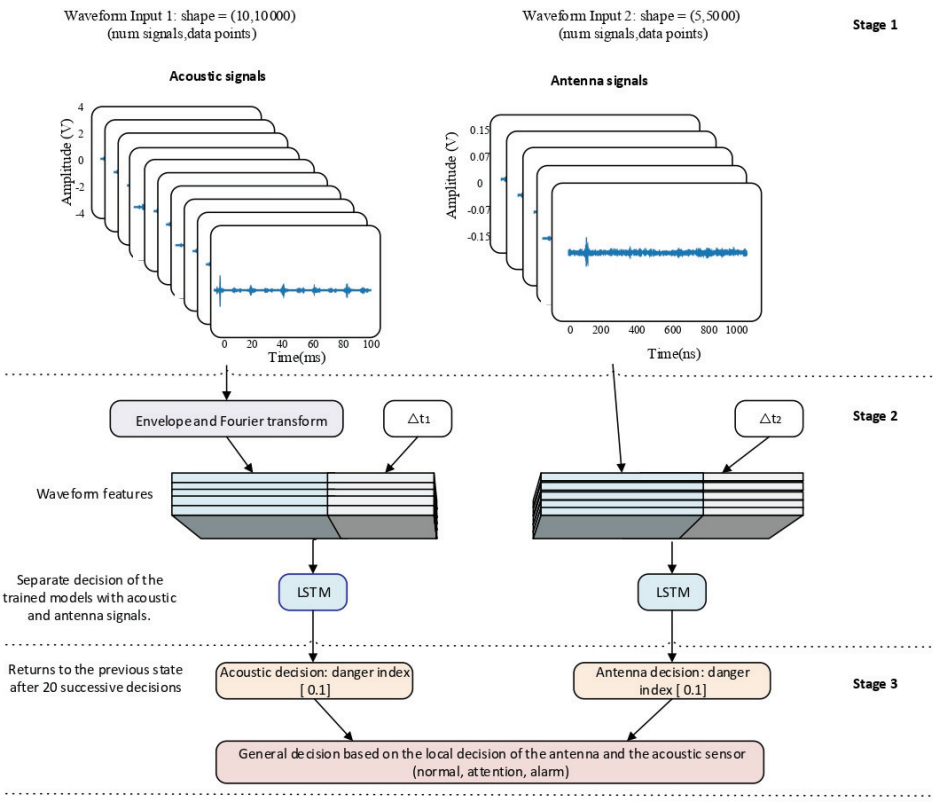

Fig. 5. Scheme of operation of the general decision system from the local prediction provided by the acoustic model and UHF.

TABLE III

RULES ESTABLISHED TO DETERMINE THE GENERAL RESPONSE OF THE ALERT SYSTEM BASED ON THE LOCAL STATES OF EACH MODEL

UHF model	Acoustic model	General Response of the system
Normal	Normal	0
Normal	Attention	0
Normal	Alarm	1
Attention	Normal	0
Attention	Attention	1
Attention	Alarm	1*
Alarm	Normal	1
Alarm	Attention	1*
Alarm	Alarm	2

normal type to go down to this state from the state of alarm. According to the logic established in Table III, the alarm state in the general response of the system only occurs when both models are in an alarm state. However, if a greater sensitivity in the response provided by the general system is desired, this logic can be adjusted, such as going to a general alarm state if one of the models is in an alarm state and the other goes to a state of attention (*). These changes will depend on how the PD activity in the insulator evolves since if the general alarm state is activated for different local states, then the system response may fluctuate each time the PD activity decreases due to the decrease in the humidity.

It is important to highlight that *P*, the decision thresholds and the logic used to establish the system response, must be adjusted for each type of insulator and the behavior of the sensors, and according to the degree of sensitivity desired in the different local and general alert states (critical systems will require greater sensitivity so that alert states are not so close to flashover).

IV. RESULTS

This section presents the results obtained for different measurement processes carried out on a 34.5-kV class ceramic insulator. For each experimental series, the insulator was periodically contaminated with saline solution through a manual spray pump remotely activated far away from the test area in order to avoid any electrical risk. Once the measurement process was finished, moments after the flashover occurred, the insulator was removed, carefully washed, and completely checked in order to identify if there was any anomalies on the surface as a result of the failure. If any type of damage was observed, the insulator was replaced with an identical one. The first part of this section explains the results obtained offline from ten different experimental series using the training and decision criteria established in Section III-B. In the second part of this section, the results for 17 new measurement processes are shown, but using the general decision system online.

A. *Offline Tests With the General Decision System*

1) Signals Label for Classification: During the different measurement processes carried out in each of the experimental series, it was observed that the acoustic sensor allowed for continuous capture of the acoustic emissions coming from the PD, these being more intense at the end of each experiment when the flashover was about to be generated. It was also observed that the antenna was much more sensitive when it

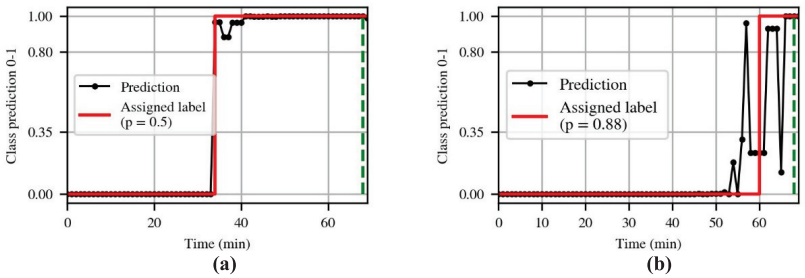

Fig. 6. Test example for (a) UHF model and (b) acoustic model.

came to capturing the electromagnetic emissions generated in the initial and intermediate stages of the contamination process. Another relevant aspect, which was recurrent during most of the experimental measurements, is that contrary to the acoustic sensor, the sensitivity of the antenna decreased during flashover when the voltage in the failure zone tried to follow or assume the network frequency. Given this behavior in both sensors during the different states of the measurement process, it was established that the information captured by the antenna would be used to try to establish the first state of alert in the general decision system, while the information delivered by the acoustic sensor would be used to try to generate the alert state that was closest to the flashover. After an iterative analysis during the training and testing of the models applying different values of P in each sensor, it was found that the most reasonable results were obtained with P between 50% and 60% for the UHF measurements and, for the measurements with the acoustic sensor, P between 75% and 90%. With these values, it was possible to obtain reasonable results where the ANNs started with small decision values (danger index) and then increased progressively as the salt deposit in the insulator also increased. For the experimental results presented in this first part, P = 50% was established for the UHF model and P = 88% for the acoustic model. The objective of maintaining a higher P value for the acoustic model is to have one of the system alert states closer to flashover while also decreasing the possibility of alarm activation in early or intermediate states of the measurement process in the event that a PD occurs, which generates a high content of acoustic emissions. In this way, the acoustic sensor also fulfills the function of complementing and/or reinforcing the alert states generated from the UHF model.

Fig. 6 shows, as an example, the test carried out in series 1 (after the training and validation process with other experimental series) from the information obtained with both sensors by applying P = 50% for the UHF model and P = 88% for the acoustic model. The red line corresponds to the labels assigned to the signals or the ground truth, and in black, the classification of the ANN models. The green vertical line corresponds to the time when the flashover occurred in the experimental series ($t_{\max}$).

Due to the stochastic behavior of PD activity in each measurement process, it is normal for the ANN predictions to oscillate throughout the experiment. This oscillatory behavior, visible in both figures, can have various causes. A frequent situation in intermediate and final states occurs when water droplets suspended on the insulator surface partially coalesce, causing partial electrical discharges (even visible and audible) that do not always end in flashover and disappear as the moisture evaporates. Under these circumstances, the acoustic and electromagnetic emissions may intensify momentarily, and both models may mistakenly interpret this as a high probability of flashover when it does not actually occur. Another common scenario that generates oscillations is when PD activity evolves due to increasing contamination, and after a spray cycle, the impact of water displaces the salt deposit on the surface. This causes a slight decrease in the surface conductivity and a change in discharge behavior. As these situations are random, it is not possible to control them experimentally; therefore, Section III-C introduces hysteresis, which precisely attenuates these oscillations without compromising the early detection of flashover.

2) General System Response: Fig. 7 shows the results obtained for the ten measurement processes with the UHF model (left), the acoustic model (middle), and the alert system (right). In black the prediction of the model, and in red the ground truth. As previously indicated, oscillations in the classification are observed in the response of both models, maintaining greater variability in the response of the acoustic model. Thanks to the hysteresis applied to the general response of the system (see Stage 3 in Section III-C), it was possible to obviate the oscillatory behavior given by the local response of the models. Exceptionally, for experiment 5, the applied hysteresis was not enough; for this case, the alarm state was generated at three different moments before the flashover. A simple solution to minimize these overshoots could be to adjust the system response so that the alarm does not return to a previous state once it is activated. However, it is desirable and convenient for the system to be able to return to a previous state of alert at any time, adequately adjusting to situations that may arise under normal operating conditions, such as the washing process of an insulator with a high degree of contamination or when it rains outside and the insulator loses part or all of its surface contamination, thus minimizing or eliminating PD activity on its surface. Under these circumstances, it is then appropriate that the system be able to respond by also lowering the alert level to a previous or initial state.

As shown in Fig. 7, the UHF model generates an alarm signal for all experiments in early or intermediate states of the contamination process, adjusting to what was stipulated during training. In terms of maintenance, the advantage of having an early warning like this is that it provides more time to plan the maintenance of the insulator and a greater margin

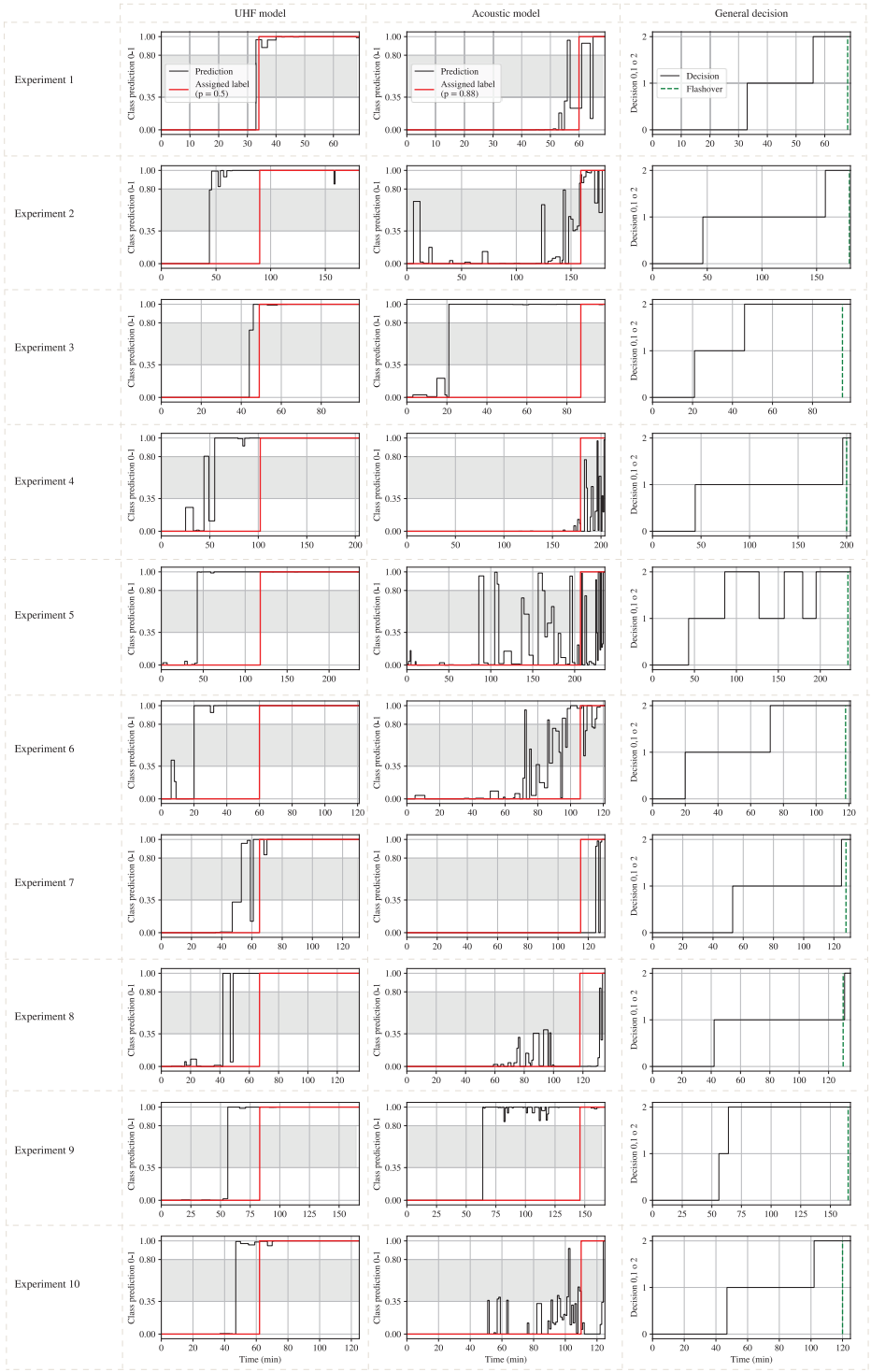

Fig. 7. Results obtained for offline tests. UHF model (left), acoustic model (middle), and general system decision (right).

of maneuver in case it is located in remote or difficult-to-access areas. On the other hand, by applying $P = 88\%$ to the acoustic model during the training stage, it was possible to generate an alarm signal with this model sometime after the UHF model, adjusting to the need to establish a second state of alert near the flashover. Only for experiment 3, the transition to the state of attention (1) in the alert system was given by the alarm delivered by the acoustic model. Probably, in that period of time, the acoustic emissions were very high, or a greater number of PDs were generated, which led the model to interpret this as a high probability of flashover, anticipating the response of the UHF model, which responded 26.72 min later (see Δt_{1-2} in Table IV).

Table IV shows, for each experimental series, Δt_1, which corresponds to the time in minutes, which elapses from the first time the state of attention (1) is issued in the general

TABLE IV

TEMPORAL PARAMETERS ASSOCIATED WITH THE ATTENTION AND ALARM STATES REGARDING THE OCCURRENCE OF FLASHOVER FOR OFFLINE MEASUREMENTS

Experiment	ΔT_1 (MIN)	ΔT_2 (MIN)	$\Delta t_{1\text{-}2}$ (min)	$\overline{\Delta t_{1-2}}$
1	34.0	11.94	22.06	0.32
2	133.45	21.65	111.8	0.62
3	**73.45 (acoustic sensor)**	**46.73**	**26.72**	**0.28**
4	155.58	3.31	152.27	0.76
5	189.36	146.72	42.64	0.18
6	97.02	45.54	51.48	0.44
7	74.51	2.2	72.31	0.56
8	87.3	-2.85	90.51	0.69
9	108.88	100.11	8.77	0.05
10	72.07	17.04	55.03	0.46
Mean	**102.56**	**39.24**	**63.32**	**0.44**

system until reaching t_{max}; Δt_2, which is the time that elapses between the instant the alarm state (2) is issued for the first time in the general system and t_{max}; and Δt_{1-2}, which is the time difference between both states and $\overline{\Delta t}_{1-2}$, which represents the normalized value of Δt_{1-2} with respect to t_{max} of each experimental series. This last value is relevant when evaluating how far apart the alarm states were delivered by both models. The value of $\overline{\Delta t}_{1-2}$ close to 1 indicates a large time difference between Δt_1 and Δt_2, and a value close to zero will indicate that the response of both models was very close. For example, when analyzing, in Fig. 7, the general response of the system in each experimental series, it is observed that in experiment 9, the alarm states of both models were very close, which is concurrent when comparing the values of $\overline{\Delta t}_{1-2}$ in Table IV, since the lowest value is obtained precisely for the experimental series 9 (0.05).

Other values of interest are the times of Δt_2 for experiments 4, 7, and 8 where the response of the acoustic model and, therefore, the general response of the system tends to be very close to flashover, that is, 3.31 min before for experiment 4, 2.2 min before for experiment 7, and 2.85 min after for experiment 8. Although, in these series, the response of the acoustic model was not very effective in terms of prediction (as it activates the alarm state in the system almost at the same time of the insulator failure), the general system fulfills the purpose of generating an early warning since, in all the experiments, it can be clearly observed that at least one state of attention is identified before flashover occurs, and in most experiments, the system establishes two alert states before flashover occurs.

When considering these results in practical field applications, it is advisable to perform insulator washing once the system enters the attention state, as the transition to the alarm state significantly increases the probability of flashover, reducing the available response time for maintenance planning. It should be noted that all these results correspond to accelerated contamination processes; therefore, the times obtained would become weeks, months, or years instead of minutes.

TABLE V

PERFORMANCE OF THE PROPOSED METHODS

Model	PRECISION ± STD	RECALL ± STD	Acc ± std
UHF	76.0 ± 12.2	99.8 ± 0.20	82.6 ± 8.01
Acoustic	59.8 ± 17.9	68.4 ± 22.9	80.2 ± 13.0

Table V presents the precision, recall, and accuracy results obtained by cross-validation for the UHF and acoustic models based on five folds during training. The UHF model demonstrated a high recall, indicating a high positive case detection rate and a low FN rate in the predictions. However, the precision showed a tendency to classify some signals labeled as "low risk" as "high risk," especially near the label threshold.

Regarding the acoustic model, oscillations were observed in the predictions, which affected the evaluation metrics. These oscillations translated into a decrease in correctly identified cases (TP) and an increase in misclassified cases (FN and FP) since some negative signals were classified as positive or vice versa. Nevertheless, the acoustic model was able to identify the risk of flashover in the final stage of each experiment. Finally, the standard deviation reported for each metric was calculated from the results obtained in each fold.

B. Implementation and Online Tests of the General Decision System

For the online application of the flashover alert system, a computer was used that integrated Python 3.6 and LabVIEW 2018 as programming platforms. The acquisition of the signals was commanded through a graphical interface implemented in LabVIEW, which was constantly in communication with the ANN models developed in Python and with the two acquisition systems that digitized the information from the sensors (NI USB-5133 and DSOS804a oscilloscope). For the training of the ANN models, five experimental series of those generated for the previously described offline tests were used. During the training, the only variation made with respect to the offline tests corresponds to the P value used in the acoustic model, which was reduced to 75%. This reduction was made in order to assess whether the acoustic model with a lower P value was capable of more quickly validating the alarm state delivered by the UHF model and, thus, preventing the alarm state in the general system from occurring too close to flashover. The P value for the UHF model was kept at 50%.

Once the training process in both models was finished, 17 new measurement processes were carried out, where it was possible to observe, in soft-real time for each experimental series, the response of the acoustic model, UHF, and the response of the general decision system. For these new measurements, the same decision thresholds used in the offline tests were maintained but modifying one of the logic criteria that governed the general response of the decision system. Specifically, a second case was established in which the system could go into an alarm state (2): if the UHF model was in alarm and the acoustic model went into the attention state. In this way, the alarm state (2) was now established for two different conditions. The idea of this modification is to give

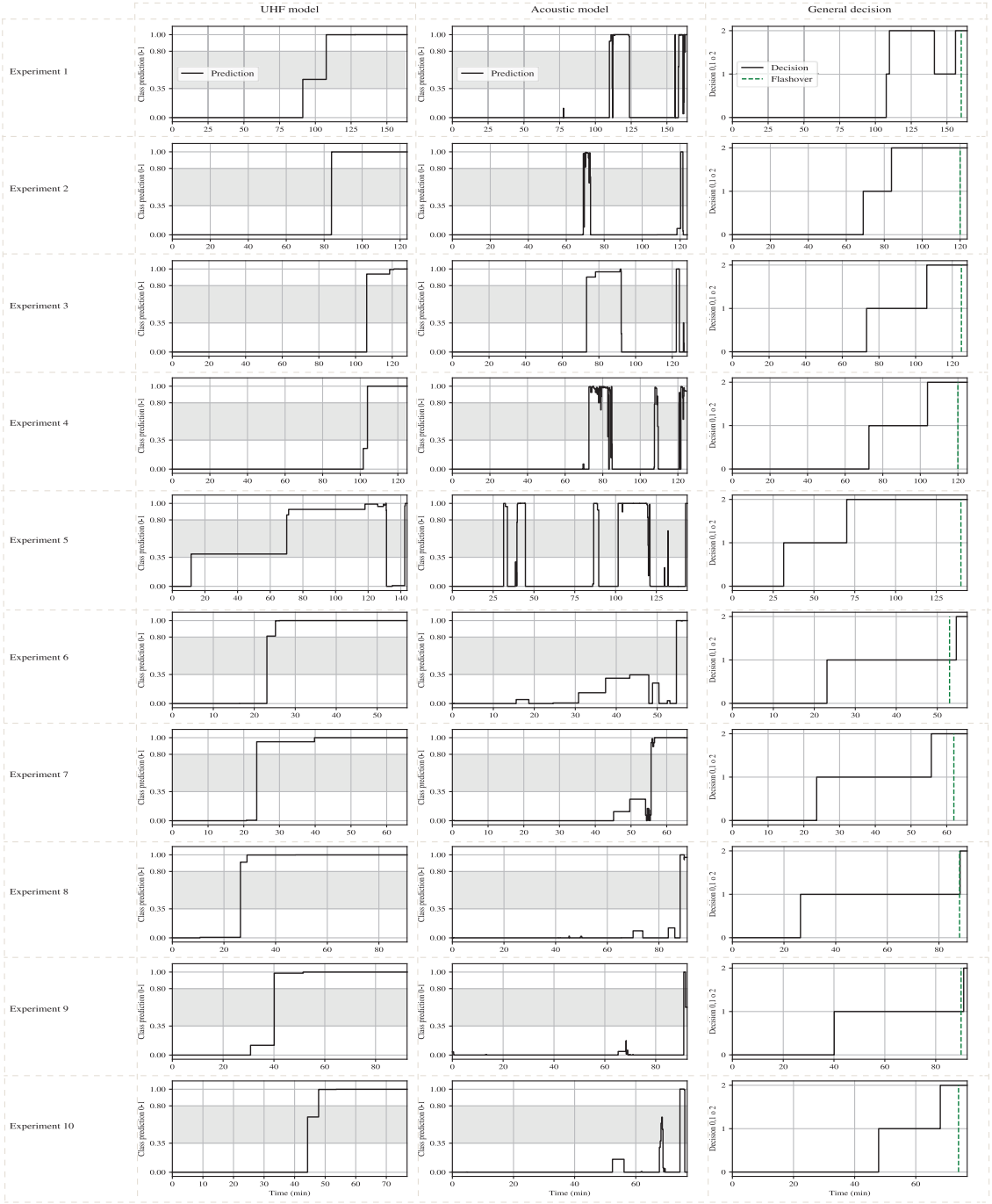

Fig. 8. Online results obtained for the UHF model (left), acoustic model (middle), and general decision system (right) for experiments 1–10.

more weight to the response provided by the acoustic model so that the system has greater sensitivity when it comes to going into a state of general alarm.

During the 17 measurement processes, the spray was applied under two different conditions. In the first five experimental series, the spraying was carried out with the same frequency used in the offline tests, that is, every 3 min. For subsequent series, the spraying frequency was increased to every 2 min. This change allowed evaluating the performance of the system under a different condition from the training. The increase in spraying frequency also accelerated the contamination process, reducing the duration of the experiments and allowing a more rapid evaluation of the performance of the system against different operating conditions. This is validated by observing, in Figs. 8 and 9, the duration time of the first five experiments with respect to the other experiments where the spraying frequency was higher. Similarly, when analyzing, in Table VI, the average of Δt_1 and Δt_2 for the two spraying conditions, it is evident that both parameters also decrease considerably with the increase in spraying frequency (the average of Δt_1 went from 61.93 to 38.61 min, and for the state of alarm, the average of Δt_2 went from 37.89 to 11.38 min).

It is interesting to observe that in effect, by training the acoustic model to activate the alarm state earlier (P = 75%),

Fig. 9. Online results obtained for the UHF model (left), acoustic model (center), and general decision system (right) for experiments 11–17.

the time difference between the alarm states generated by both models can be reduced. In this way, for most of the measurement processes, the acoustic model was able to validate the danger condition delivered by the UHF model faster and even earlier. As observed in Table VI, the mean of $\overline{\Delta t}_{1-2}$ in the two groups with different spraying frequencies is much lower than that obtained in the offline tests (see Table IV). Note that although the frequency of spraying in the first five experimental series is the same as that used in the offline measurements, the mean value of $\overline{\Delta t}_{1-2}$ decreased considerably from 0.44 to 0.18. Even in experimental measurements 2, 3, 4, 5, 11, and 13, the attention state was first activated by the alarm response generated by the acoustic model. Only in the experimental series 6, 8, 9, and 14, the alarm response in the acoustic sensor was slightly late, being activated very close to flashover. These results confirm that the hybrid architecture employed in both models is capable of extracting important features from PD signals that are directly related to the evolution of PD activity as the salt deposition in the insulator increases, regardless of the duration of the experiment or the way in which the contamination in the insulator evolves.

Finally, experimental series 12 and 15 were carried out, with the insulator left clean for approximately 1 hour without spraying. Since, under this condition, there is no significant activity of PDs or it is practically null, it can be confirmed that the system responds adequately and remains in the normal state during the entire time that the two experiments last.

C. Adaptability and Implementation Challenges for Field Deployment

The results obtained under controlled laboratory conditions confirm that the proposed hybrid UHF-acoustic architecture successfully anticipates flashover in 34.5-kV ceramic

TABLE VI

TEMPORAL PARAMETERS ASSOCIATED WITH ATTENTION AND ALARM STATES REGARDING THE OCCURRENCE OF FLASHOVER FOR ONLINE MEASUREMENTS MADE WITH DIFFERENT SPRAYING FREQUENCIES

Experiment	ΔT_1 (MIN)	ΔT_2 (MIN)	$\Delta t_{1\text{-}2}$ (min)	$\overline{\Delta t_{1-2}}$
1	51.88	49.70	2.18	0.01
2	50.6	36.05	14.55	0.12
3	51.68	18.43	33.25	0.26
4	47.12	15.81	31.31	0.26
5	108.41	69.49	38.92	0.27
Mean	**61.93**	**37.89**	**23.60**	**0.18**
6	29.64	-1.90	31.54	0.59
7	38.3	6.09	32.21	0.51
8	61.6	-0.23	61.83	0.70
9	49.83	-1.40	51.23	0.56
10	25.96	5.86	20.1	0.27
11	29.47	8.70	20.77	0.31
12	--	--	--	--
13	8.83	2.03	6.8	0.08
14	36.37	0.39	35.98	0.49
15	--	--	--	--
16	43.87	38.19	5.68	0.08
17	62.26	56.07	6.19	0.05
Mean*	**38.61**	**11.38**	**27.23**	**0.36**

* Experimental series 12 and 15 are not taken into account for this calculation.

insulators through a flexible logic based on thresholds, temporal hysteresis, and general decision rules. Practical adaptation of the system to other scenarios can be achieved through software recalibration without redesigning sensor hardware by adjusting the following four parameter sets:

1) the temporal percentage P, which defines the point from which signals are labeled as high risk during training;
2) thresholds applied to the indices $f^*(x)$ and $g^*(x)$, determining the local alert states: normal, attention, and alarm;
3) temporal hysteresis used to stabilize the system response, balancing sensitivity and stability, and smoothing transitions between levels;
4) decision rules (summarized in Table III) combine local states to establish the general alert state of the system clearly and consistently.

However, implementing this system in real operational conditions necessitates considering and overcoming specific technical challenges beyond those addressed in laboratory configurations. These four parameter sets must be carefully adjusted to compensate for significant variations in repetition rate and the time–frequency behavior of PD when key aspects such as insulator material, geometry, voltage level, surface contamination type, and environmental conditions change.

The geometry and material of the insulator significantly impact PD characteristic patterns. Ceramic and glass insulators predominantly feature hydrophilic surfaces, favoring the formation of continuous conductive films under high humidity conditions, promoting distributed PD activity over virtually the entire surface. Conversely, polymeric insulators possess hydrophobic properties, generally limiting conductive point formation; however, under severe conditions or prolonged exposure to contaminants and moisture, this hydrophobicity can be partially reduced, facilitating localized, and high-intensity discharges in specific areas [4], [38].

Moreover, the diversity of contaminants present in real environments considerably increases the complexity of the problem. In industrial or mining environments, contaminants such as dust and soot substantially modify insulator surface resistivity, thereby altering electromagnetic and acoustic radiation patterns associated with PD sources. In rural areas, seasonal factors such as pollen and bird droppings generate specific points of high conductivity, whereas, in polar environments, ice formation could notably affect acoustic and electromagnetic wave propagation due to induced variations in the dielectric constant and acoustic properties [2], [6], [16].

In addition, field implementation entails significant electromagnetic and acoustic noise levels, especially in industrial areas with continuous machinery operation. To effectively manage these challenges, it is essential to conduct rigorous characterization processes and establish site-specific baseline profiles, allowing precise definition of thresholds and parameters adapted to local conditions. Consequently, although the proposed system has demonstrated flexibility and robustness under controlled laboratory conditions, its effective implementation in diverse operational contexts requires further adjustment of the aforementioned parameters, along with specific validation and adaptation processes, depending on insulator material, geometry, voltage level, contamination type, and particular environmental conditions of the site. These specific adjustments will ensure system reliability and accuracy under real operating conditions.

V. CONCLUSION

This article presents an innovative insulator flashover alert system based on the measurement of acoustic and UHF emissions produced by PD activity on the surface of contaminated insulators. The system uses two ANN models with a hybrid CNN-LSTM architecture to generate three general alert states (normal, attention, and alarm). It is important to highlight that this system can be easily adapted to any type of insulator, as long as it is previously adjusted according to the evolution of the PD activity in the insulator. As indicated in Section IV, such adjustment will require carrying out several contamination and measurement processes with a similar insulator to the one to be monitored.

The experimental results obtained during the measurement processes showed that the UHF model performed better when establishing initial alert states, while the acoustic model had a better performance when it came to establishing the states of alarm close to flashover. For this reason, for the training of the models both in the offline tests and in the online tests, a higher P value was established in the acoustic model. By evaluating the behavior of the system for different P values, it was possible to validate the capacity of the implemented hybrid architecture to identify or relate specific patterns of PD signals for certain stages throughout the contamination

process. In general, it was observed that in the measurement processes where the P value was reduced during the training of the acoustic model, a decrease in the time difference between the alarm states generated by both models was also produced.

The response of the system in each of the experimental measurements started from the normal condition, going through a state of attention, to finally reach an alarm state. In the case of offline measurements, in nine of the ten experimental series carried out, the system managed to deliver the two alarm states before the flashover was generated, while, for the online measurements, the two alarm states were established in 12 of the 15 experimental series. Despite the fact that the alarm state failed in 4 of the 25 cases evaluated, in all the experimental series, the purpose of generating an early warning for all the measurement processes was fulfilled since at least one of the models generated a state of attention before the flashover occurred. It is important to highlight that these results can also vary significantly depending on the adjustment made to the decision thresholds that classify the danger indices and the decision logic established with the local response of the models. By appropriately modifying these parameters, it is possible to adjust the response sensitivity when establishing the local alert states of the models or the general response of the alert system.

Although precisely predicting the flashover time was beyond the scope of this work, the deep learning approach adopted provides a foundation for developing new insulation monitoring systems using low-cost sensors that do not require galvanic contact with the equipment.

Future research should focus on systematically determining these adjustment parameters for diverse insulator types and practical field scenarios, ensuring that the presented methodology maintains its robustness, accuracy, and early-warning effectiveness beyond the controlled laboratory environment.

REFERENCES

[1] N. Hashemnia, A. Abu-Siada, and S. Islam, "Detection of power transformer bushing faults and oil degradation using frequency response analysis," *IEEE Trans. Dielectr. Electr. Insul.*, vol. 23, no. 1, pp. 222–229, Feb. 2016.

[2] A. A. Salem et al., "Pollution flashover voltage of transmission line insulators: Systematic review of experimental works," *IEEE Access*, vol. 10, pp. 10416–10444, 2022.

[3] J. T. Gorur, R. S. Cherney, and E. A. Burnham, *Outdoor Insulators*. Phoenix, AZ, USA: Ravi S. Gorur, 1999.

[4] S. Polisetty, A. El-Hag, and S. Jayram, "Classification of common discharges in outdoor insulation using acoustic signals and artificial neural network," *High Voltage*, vol. 4, no. 4, pp. 333–338, Dec. 2019.

[5] Z. Yang, X. Jiang, Z. Zhang, D. Zhang, and Y. Liu, "Study on the influence rules of soluble contaminants on flashover voltage of disc suspension insulators," *IEEE Trans. Dielectr. Electr. Insul.*, vol. 23, no. 6, pp. 3523–3530, Dec. 2016.

[6] S. Zhao, X. Jiang, Z. Zhang, J. Hu, and L. Shu, "Flashover voltage prediction of composite insulators based on the characteristics of leakage current," *IEEE Trans. Power Del.*, vol. 28, no. 3, pp. 1699–1708, Jul. 2013.

[7] L. Cui, R. S. Gorur, and D. Chipman, "Evaluating flashover performance of insulators under fire fighting conditions," *IEEE Trans. Dielectr. Electr. Insul.*, vol. 24, no. 2, pp. 1051–1056, Apr. 2017.

[8] H. R. Sezavar, N. Fahimi, and A. A. Shayegani, "A dynamic intelligent approach based on Gaussian function for prediction of the flashover voltage conditions on polluted polymer insulators," *IEEE Trans. Power Del.*, vol. 37, no. 5, pp. 3458–3468, Oct. 2022.

[9] S. Frizzo Stefenon, M. C. Silva, D. W. Bertol, L. H. Meyer, and A. Nied, "Fault diagnosis of insulators from ultrasound detection using neural networks," *J. Intell. Fuzzy Syst.*, vol. 37, no. 5, pp. 6655–6664, Nov. 2019.

[10] J. M. de Barros Bezerra, A. M. N. Lima, G. S. Deep, and E. G. da Costa, "An evaluation of alternative techniques for monitoring insulator pollution," *IEEE Trans. Power Del.*, vol. 24, no. 4, pp. 1773–1780, Oct. 2009.

[11] C.-Y. Huang, C.-S. Kuo, and S.-P. Luan, "Evaluation and application of bounded generalized Pareto analysis to fault distributions in open source software," *IEEE Trans. Rel.*, vol. 63, no. 1, pp. 309–319, Mar. 2014.

[12] A. Nuñez, A. Jamshidi, and H. Wang, "Pareto-based maintenance decisions for regional railways with uncertain weld conditions using the Hilbert spectrum of axle box acceleration," *IEEE Trans. Ind. Informat.*, vol. 15, no. 3, pp. 1496–1507, Mar. 2019.

[13] S. A. V. Wiel and L. G. Votta, "Assessing software designs using capture-recapture methods," *IEEE Trans. Softw. Eng.*, vol. 19, no. 11, pp. 1045–1054, Nov. 1993.

[14] J. Ramírez-Niño and A. Pascacio, "Acoustic measuring of partial discharge in power transformers," *Meas. Sci. Technol.*, vol. 20, no. 11, Oct. 2009, Art. no. 115108.

[15] R. J. Villalobos, L. A. Moran, F. Huenupán, F. Vallejos, R. Moncada, and C. Pesce G.,, "A new current transducer for on-line monitoring of leakage current on HV insulator strings," *IEEE Access*, vol. 10, pp. 78818–78826, 2022.

[16] N. F. Sopelsa Neto, S. F. Stefenon, L. H. Meyer, R. G. Ovejero, and V. R. Q. Leithardt, "Fault prediction based on leakage current in contaminated insulators using enhanced time series forecasting models," *Sensors*, vol. 22, no. 16, p. 6121, Aug. 2022.

[17] Z. Ghiasi, F. Faghihi, and A. A. Shayegani-Akmal, "Artificial neural network approach for prediction of leakage current of polymeric insulator under non-uniform fan-shaped contamination," *Electr. Power Syst. Res.*, vol. 209, Aug. 2022, Art. no. 107920.

[18] H. Y. He, Z. Zhang, W.-J. Lee, Y. Cao, D. Luo, and T. Lu, "A contactless insulator contamination levels detecting method based on infrared images features and RBFNN," in *Proc. IEEE Ind. Appl. Soc. Annu. Meeting (IAS)*, Sep. 2018, pp. 1–9.

[19] L. Liu, H. Mei, C. Guo, Y. Tu, and L. Wang, "Pixel-level classification of pollution severity on insulators using photothermal radiometry and multiclass semisupervised support vector machine," *IEEE Trans. Ind. Informat.*, vol. 17, no. 1, pp. 441–449, Jan. 2021.

[20] A. Abedini-Livari, K. Firuzi, and M. Vakilian, "Distinguishing polymeric insulators PD sources through RF PD measurement," *IET Gener., Transmiss. Distrib.*, vol. 14, no. 21, pp. 4859–4865, Nov. 2020.

[21] W. Si, H. Guan, W. Yao, C. Fu, and P. Yuan, "Combined in-oil PD sensor with AE and UHF methods for PD detection in transformer," *Energy Rep.*, vol. 8, pp. 177–191, Aug. 2022.

[22] S. A. Kashinath et al., "Review of data fusion methods for real-time and multi-sensor traffic flow analysis," *IEEE Access*, vol. 9, pp. 51258–51276, 2021.

[23] K. Liu, N. Z. Gebraeel, and J. Shi, "A data-level fusion model for developing composite health indices for degradation modeling and prognostic analysis," *IEEE Trans. Autom. Sci. Eng.*, vol. 10, no. 3, pp. 652–664, Jul. 2013.

[24] X. Lin et al., "Natural insulator contamination test results on various shed shapes in heavy industrial contamination areas," *IEEE Trans. Electr. Insul.*, vol. 27, no. 3, pp. 593–600, Jun. 1992.

[25] B. Cao, L. Wang, and F. Yin, "A low-cost evaluation and correction method for the soluble salt components of the insulator contamination layer," *IEEE Sensors J.*, vol. 19, no. 13, pp. 5266–5273, Jul. 2019.

[26] L. Orellana, G. Avaria, J. Ardila-Rey, S. Davis, R. Schurch, and C. Pavez, "Inference of X-ray emission from a plasma focus discharge: Comparison between characteristic parameters and neural network analyses," *IEEE Access*, vol. 8, pp. 79273–79286, 2020.

[27] Z. Li, N. Qu, X. Li, J. Zuo, and Y. Yin, "Partial discharge detection of insulated conductors based on CNN-LSTM of attention mechanisms," *J. Power Electron.*, vol. 21, no. 7, pp. 1030–1040, Jul. 2021.

[28] Z. Zhi, L. Liu, D. Liu, and C. Hu, "Fault detection of the harmonic reducer based on CNN-LSTM with a novel denoising algorithm," *IEEE Sensors J.*, vol. 22, no. 3, pp. 2572–2581, Feb. 2022.

[29] M. Alhussein, K. Aurangzeb, and S. I. Haider, "Hybrid CNN-LSTM model for short-term individual household load forecasting," *IEEE Access*, vol. 8, pp. 180544–180557, 2020.

[30] I. Goodfellow, Y. Bengio, and A. Courville, *Deep Learning*. Cambridge, MA, USA: MIT Press, 2016.

[31] Y. Lecun, L. Bottou, Y. Bengio, and P. Haffner, "Gradient-based learning applied to document recognition," *Proc. IEEE*, vol. 86, no. 11, pp. 2278–2323, 1998.
[32] S. Hochreiter and J. Schmidhuber, "Long short-term memory," *Neural Comput.*, vol. 9, no. 8, pp. 1735–1780, Nov. 1997.
[33] J. Heaton, "Ian Goodfellow, Yoshua Bengio, and Aaron Courville: Deep learning," *Genet. Program. Evolvable Mach.*, vol. 19, pp. 305–307, 2018, doi: 10.1007/s10710-017-9314-z.
[34] L. Orellana, J. Ardila-Rey, G. Avaria, and S. Davis, "Danger assessment of the partial discharges temporal evolution on a polluted insulator using UHF measurement and deep learning," *Eng. Appl. Artif. Intell.*, vol. 124, Sep. 2023, Art. no. 106573.
[35] F. Karim, S. Majumdar, H. Darabi, and S. Chen, "LSTM fully convolutional networks for time series classification," *IEEE Access*, vol. 6, pp. 1662–1669, 2018.
[36] V. Nair and G. E. Hinton, "Rectified linear units improve restricted Boltzmann machines," in *Proc. 27th Int. Conf. Mach. Learn.*, 2010, pp. 807–814.
[37] N. Srivastava, G. E. Hinton, A. Krizhevsky, I. Sutskever, and R. Salakhutdinov, "Dropout: A simple way to prevent neural networks from overfitting," *J. Mach. Learn. Res.*, vol. 15, no. 1, pp. 1929–1958, 2014.
[38] S. Chandrasekar, C. Kalaivanan, A. Cavallini, and G. Montanari, "Investigations on leakage current and phase angle characteristics of porcelain and polymeric insulator under contaminated conditions," *IEEE Trans. Dielectr. Electr. Insul.*, vol. 16, no. 2, pp. 574–583, Apr. 2009.